

Pan-flavivirus analysis reveals sfRNA-independent, 3'UTR-biased siRNA production from an Insect-Specific Flavivirus

3

Benoit Besson^{a}, Gijs J. Overheul^a, Michael T. Wolfinger^{b,c,d} Sandra Junglen^e, Ronald P. van Rij^a*

6

⁷ ^aDepartment of Medical Microbiology, Radboud University Medical Center, Nijmegen, The
⁸ Netherlands

⁹ ^bResearch Group Bioinformatics and Computational Biology, Faculty of Computer Science,
¹⁰ University of Vienna, Vienna, Austria.

11 ^cDepartment of Theoretical Chemistry, University of Vienna, Vienna, Austria.

12 dRNA Forecast e.U., Vienna, Austria.

13 ^eInstitute of Virology, Charité-Universitätsmedizin Berlin, Corporate Member of Free
14 University, Humboldt-University and Berlin Institute of Health, Berlin, Germany.

15

16 Running title: Mosquito RNAi responses to flaviviruses

17 #Correspondence to Ronald P. van Rij, ronald.vanrij@radboudumc.nl

18 *Present address: Benoit Besson, Université de Strasbourg, RNA architecture and reactivity
19 & Insect Models of Innate Immunity, Institut de Biologie Moléculaire et Cellulaire, CNRS,
20 Strasbourg, France.

21 Benoit Besson and Gijs J Overheul contributed equally to this work. Author order was
22 determined alphabetically.

23

24 Word count abstract: 249

25 Word count text: 5165 (excluding references and figure legends)

26 ABSTRACT

27 RNA interference (RNAi) plays an essential role in mosquito antiviral immunity, but it is not
28 known whether viral siRNA profiles differ between mosquito-borne and mosquito-specific
29 viruses. A pan-Orthoflavivirus analysis in *Aedes albopictus* cells revealed that viral siRNAs
30 were evenly distributed across the viral genome of most representatives of the *Flavivirus*
31 genus. In contrast, siRNA production was biased towards the 3' untranslated region (UTR) of
32 the genomes of classical insect-specific flaviviruses (cISF), which was most pronounced for
33 Kamiti River virus (KRV), a virus with a unique, 1.2 kb long 3' UTR. KRV-derived siRNAs
34 were produced in high quantities and almost exclusively mapped to the 3' UTR. We mapped
35 the 5' end of KRV subgenomic flavivirus RNAs (sfRNAs), products of the 5'-3'
36 exoribonuclease XRN1/Pacman stalling on secondary RNA structures in the 3' UTR of the
37 viral genome. We found that KRV produces high copy numbers of a long, 1017 nt sfRNA1
38 and a short, 421 nt sfRNA2, corresponding to two predicted XRN1-resistant elements.
39 Expression of both sfRNA1 and sfRNA2 was reduced in *Pacman* deficient *Aedes albopictus*
40 cells, however, this did not correlate with a shift in viral siRNA profiles. We suggest that
41 cISFs and particularly KRV developed a unique mechanism to produce high amounts of
42 siRNAs as a decoy for the antiviral RNAi response in an sfRNA-independent manner.

43

44 IMPORTANCE

45 The *Flavivirus* genus contains diverse mosquito viruses ranging from insect-specific viruses
46 circulating exclusively in mosquito populations to mosquito-borne viruses that cause disease
47 in humans and animals. Studying the mechanisms of virus replication and antiviral immunity
48 in mosquitoes is important to understand arbovirus transmission and may inform the
49 development of disease control strategies. In insects, RNA interference (RNAi) provides
50 broad antiviral activity and constitutes a major immune response against viruses. Comparing

51 diverse members of the *Flavivirus* genus, we found that all flaviviruses are targeted by RNAi.
52 However, the insect-specific Kamiti River virus was unique in that small interfering RNAs
53 are highly skewed towards its uniquely long 3' untranslated region. These results suggest that
54 mosquito-specific viruses have evolved unique mechanisms for genome replication and
55 immune evasion.

56

57 INTRODUCTION

58 The *Orthoflavivirus* genus constitutes diverse phylogenetic clades of viruses, found in
59 vertebrates and arthropods including mosquitoes (1). Mosquito-borne arboviruses are
60 transmitted horizontally between mosquitoes and vertebrates, whereas insect-specific
61 flaviviruses (ISF) are thought to be primarily transmitted vertically and restricted to their
62 arthropod hosts (2, 3). ISFs are further separated into two distinct phylogenetic clades:
63 lineage I or classical ISFs (cISF), a clade that branches at the base of the *Orthoflavivirus*
64 genus, and lineage II or dual-host affiliated ISFs (dISF) that forms a separate phylogenetic
65 clade embedded in vector-borne clades (4–6). While the healthcare and economic burden of
66 arboviruses is well established (7), ISFs have been proposed as modulators of arbovirus
67 transmission and are being explored for biotechnological applications such as vaccine
68 development (8–10).

69

70 Flaviviruses have an ~11 kb long, positive-sense genomic RNA ((+)gRNA), which
71 circularizes via long range RNA-RNA interactions between their 5' and 3' untranslated
72 regions (UTR) for RNA translation and replication (11, 12). Asymmetric replication is
73 mediated via an antigenomic negative-sense RNA intermediate ((-)gRNA), which serves as a
74 template for replication of the (+)gRNA and is hypothesized to be annealed either to its
75 template and/or to newly synthesized (+)gRNA, forming double-stranded RNA (dsRNA) (13,
76 14).

77 Flaviviruses take advantage of the ability of RNA to form regulatory, evolutionarily
78 conserved elements to produce a highly structured subgenomic flavivirus RNA (sfRNA) (15–
79 18). Formation of sfRNA is regulated by exoribonuclease-resistant RNA (xrRNA) structures
80 in the 3' UTR, which typically encompass three-way junctions (3WJ) or stem-loop (SL)
81 elements that adopt a particular fold, mediated by a pseudoknot (19). The tight and complex

82 structure of xrRNAs stalls the 5'-3' exoribonuclease 1 (XRN1), also referred to as Pacman in
83 mosquitoes, and terminates the degradation of viral RNA (20), resulting in the production of
84 sfRNA. Flaviviruses may encode multiple xrRNA-like structures (21), each of which can
85 induce the production of a distinct sfRNA species. While the longest sfRNA generated from
86 the first xrRNA is generally the most abundant, sfRNA production from individual xrRNAs
87 may vary between mammalian and mosquito hosts, suggesting viral adaptation to the host
88 (20, 22–24).

89 It is well established that sfRNA is essential for flavivirus replication and dissemination (16,
90 23, 25, 26), for which several mechanisms have been suggested, in some cases with sfRNA
91 serving as a decoy for the viral genome. For example, sfRNA was shown to inhibit the host
92 RNA decay pathway (27), to control apoptosis (16, 28), to encode a microRNA (29), and to
93 inhibit the mosquito Toll pathway (30). Moreover, sfRNA can be a substrate for small
94 interfering RNA (siRNA) production by Dicer (31) and was proposed to inhibit the RNA
95 interference (RNAi)-based antiviral immune response (27, 32–34), although this was recently
96 disputed (28).

97

98 Mosquitoes have an RNAi-centered immune response, and deficiency in RNAi leads to
99 increased sensitivity to virus infections (35–41). Viral dsRNA is cleaved by Dicer-2 into 21
100 nt viral siRNA duplexes (vsiRNAs), which are loaded into the Argonaute-2-containing RISC
101 complex with the help of RNA-binding proteins Loqs and R2D2 (38, 42). Upon loading the
102 duplexes, one of the RNA strands (passenger strand) is degraded and the remaining guide
103 strand is used by Argonaute-2 to recognize and cleave complementary single-stranded viral
104 RNA.

105 In addition to the siRNA pathway, the PIWI-interacting RNA (piRNA) pathway has been
106 implicated in antiviral defense in mosquitoes (38, 43, 44). In this pathway, viral single-

107 stranded RNA is processed into mature 25–30 nt viral piRNAs (vpiRNAs) associating with
108 the PIWI proteins Piwi5 and Ago3, which amplify the piRNA response in a feedforward
109 mechanism called the ping-pong amplification loop (45–47). While Piwi5 is required for
110 vpiRNA biogenesis in *Aedes aegypti* (45, 46), only *Piwi4* depletion has thus far been shown
111 to affect arbovirus replication (48, 49) and the importance of the piRNA response during
112 acute viral infections remains to be clarified. Yet, endogenous viral elements (EVE) in the
113 genome of *Aedes* mosquitoes give rise to piRNAs that can target cognate viral RNA and
114 reduce viral RNA levels, especially in the ovaries (49–52), underlining the antiviral potential
115 of the piRNA pathway.

116

117 While the RNAi response seems to be a widely active antiviral response, it is currently
118 unclear whether mosquito-borne viruses and insect-specific viruses are differentially targeted.
119 To address this question, we profiled small RNAs in *Aedes albopictus* mosquito cells infected
120 with mosquito-borne viruses and ISFs and found that while siRNAs mapped across the entire
121 length of the viral genome for all mosquito-borne flaviviruses tested, vsiRNAs were
122 predominantly derived from the 3' UTR of Kamiti River virus (KRV), a cISF originally
123 identified in *Aedes mcintoshi* mosquitoes (53). A similar, but less pronounced trend was also
124 observed for two other cISFs, Culex flavivirus (CxFV) and cell-fusing agent virus (CFAV).
125 Having noted that KRV has a particularly long 3' UTR, we set out to characterize viral
126 subgenomic RNA species and mapped two main sfRNAs regulated by two predicted
127 XRN1/Pacman-resistant xrRNA structures. Loss of *Pacman* resulted in a shift in sfRNA
128 production, but no concomitant shift in siRNA profiles, suggesting that the 3'UTR biased
129 siRNAs are produced in an sfRNA independent manner. We speculate that KRV and likely
130 other cISFs developed a unique mechanism to evade antiviral RNAi.

131

132 RESULTS

133 **RNAi response to flavivirus infection in *Aedes* mosquito cells**

134 Given the importance of the siRNA response for antiviral immunity in mosquitoes, we
135 analyzed viral small RNAs produced during flavivirus infection. Representatives of each
136 major clade of mosquito-associated flaviviruses were selected to provide a pan-flavivirus
137 overview of viral siRNA and piRNA profiles in *Ae. albopictus* U4.4 cells. Specifically, we
138 selected the *Culex*-associated arboviruses Saint-Louis encephalitis virus (SLEV, isolate MSI-
139 7) and West Nile virus (WNV), the *Aedes*-associated arboviruses dengue virus (DENV
140 serotype 2) and Zika virus (ZIKV), the dISF Nounané virus (NOUV), the *Culex*-associated
141 cISF CxFV, and the *Aedes*-associated cISFs CFAV and KRV (Fig. 1A). Further, the
142 epidemic SLEV MSI-7 strain was compared to the ancestral SLEV Pal strain as
143 representatives of cosmopolitan and enzootic viruses, respectively (54). All tested
144 flaviviruses replicated to similar levels in U4.4 cells with approximately 10^8 RNA copies/ μ g
145 of total RNA at 72 hours post infection, except for CxFV and CFAV, which reached $3\text{--}5 \cdot 10^6$
146 copies/ μ g of total RNA (Fig. S1).

147

148 As observed previously (3, 31, 45, 48, 50, 55, 56), size profiles of viral small RNAs were
149 characterized by a prominent peak of 21 nt vsiRNAs from both positive- and negative-sense
150 RNA for all tested flaviviruses (Fig. 1B), with a shoulder of predominantly positive-sense
151 RNAs of 25–30 nt. Given similar viral RNA levels (Fig. S1A), differences in scales suggest
152 that NOUV elicited an overall weaker siRNA response compared to WNV, SLEV-MSI-7/Pal,
153 DENV and ZIKV. CxFV also elicited a weaker siRNA response, which may be due to the
154 lower RNA levels (Fig. S1B). In contrast, KRV elicited the strongest siRNA response
155 recorded, and CFAV induced a strong siRNA response despite its relatively low RNA levels
156 in cells.

157

158 Although we have not formally demonstrated PIWI-protein association, the shoulder of 25–30
159 nt viral small RNAs (Fig. 1B) likely represent vpiRNAs. Indeed, the 1U-bias characteristic of
160 PIWI-associated piRNAs was detectable for 25–30 nt sized RNAs of CFAV, KRV, DENV
161 and SLEV (Fig. S2A). Moreover, a 10A-bias characteristic of piRNAs produced by ping-
162 pong amplification was detectable on positive-sense, piRNA-sized RNAs of CFAV, KRV,
163 DENV. Using the gRNA as reference, the flaviviruses differed from each other in the relative
164 amounts of 25–30 nt viral small RNAs (Fig. S1C). Notably, viral piRNA over siRNA ratios
165 were relatively low for the *Aedes*-associated arboviruses DENV and ZIKV (0.08 and 0.04,
166 respectively), whereas these ratios were higher for NOUV and CFAV (0.77 and 0.85,
167 respectively) (Fig. 1B).

168

169 **Asymmetric distribution of vsiRNAs across the KRV genome**

170 The distribution of vsiRNAs across the viral genomes (Fig. 2) showed relative uniform
171 mapping of vsiRNAs on both the (+)gRNA and (-)gRNA. A notable exception was KRV, for
172 which most vsiRNAs mapped to the 3' UTR region and presentation of the data on a
173 logarithmic scale is required to show siRNAs mapping to other parts of the genome, albeit at
174 extremely low levels (Fig. 2B). This pattern is reminiscent of 3' UTR biased mapping
175 observed for the other cISFs CxFV, CFAV and AEFV, although the skewed distribution is
176 much more pronounced for KRV (Fig. 2A and C) (3, 50, 57). About 14% of the vsiRNAs of
177 CxFV and CFAV and more than 95% of KRV vsiRNAs derived from their 3' UTRs, in stark
178 contrast to the other flaviviruses for which a median of ~4% of vsiRNAs mapped to the 3'
179 UTR (Fig. 2C).

180

181 In contrast to siRNAs, vpiRNAs mapped to several discrete hotspots on the viral (+)gRNA
182 (Fig. S2). For each virus analyzed, vpiRNAs mapped to different genome coordinates in a
183 manner that was highly reproducible in replicate experiments, in agreement with previous
184 observations (43, 48, 50, 58). It is worth noting that KRV derived piRNAs mapped at several
185 hotspot across the gRNA and were not enriched at the 3' UTR, indicating that each pathway
186 processes a different substrate. Altogether, our data illustrate a general antiviral siRNA
187 response to flaviviruses, no major differences between the ancestral and pandemic SLEV
188 strains, and highlight the unique case of cISFs, especially KRV, for which the skewed
189 distribution of vsiRNA towards the 3' UTR suggests a unique siRNA response to the
190 infection.

191

192 **KRV has a unique 3' UTR**

193 KRV has a 3' UTR of 1208 nt, much longer than in any other member of the *Flavivirus*
194 genus (median of 486 nt), but also longer than the 3' UTRs of members of the cISF clade
195 (median of 663 nt) (Fig. 3A). Structure predictions suggested that the KRV 3' UTR is highly
196 structured, comprising evolutionarily conserved elements, alongside secondary RNA
197 structures that appear to be unique to KRV (Fig. 3B). Our model predicted the signature
198 flavivirus regulatory SL at the 3' end of the genome and corroborated the presence of two
199 cISF xrRNA structures (xrRNA1 and xrRNA2) that are highly conserved between KRV,
200 CFAV and Aedes Flavivirus (AEFV), which are closely related to *Anopheles*-associated
201 cISFs (59, 60), and not conserved in the more distant Culex Flavivirus (CxFV) and
202 Xishuangbanna Aedes Flavivirus (XFV). Moreover, structure predictions of the KRV 3' UTR
203 suggested the presence of simple and branched stem-loop elements, as well as several long
204 hairpins, including the internal 3' stem-loop (i3'SL), previously predicted using a
205 comparative genomics approach (21).

206 Interestingly, while the 3' terminal 419 nt long sequence of the KRV 3' UTR downstream of
207 xrRNA2 appears to be conserved with other cISFs (21), the 5' terminal 789 nt sequence
208 extending from the stop codon to xrRNA2 appears to be unique to KRV (Fig. 3B). This 5'
209 sequence of KRV 3' UTR does not seem to share ancestry with AEFV, the cISF with the
210 second longest 3' UTR (Fig. 3A), nor with other flaviviruses, with the exception of xrRNA1
211 which is highly conserved both in structure and sequence, and was hypothesized to be the
212 result of a self-duplication event (61, 62).

213

214 **KRV produces multiple subgenomic flavivirus RNA species**

215 Given the long KRV 3' UTR and the observation that flavivirus 3' UTRs give rise to
216 sfRNAs, we visualized the RNA species produced during KRV infection of *Ae. albopictus*
217 U4.4 cells by northern blot (Fig. 3C left panel). Two sfRNA (sfRNA1 and sfRNA2) were
218 detected, likely the product of XRN1/Pacman stalling on xrRNA structures. Both sfRNAs
219 were displayed strong signals corresponding to the expected sizes (~1000 and ~400 nt),
220 suggesting that KRV sfRNA1 and sfRNA2 greatly outnumber KRV (+)gRNA, as observed
221 for other flaviviruses as well (16, 28, 31). When quantifying the different KRV RNA species
222 by RT-qPCR (Fig. 3D), we found that for each molecule of gRNA, there was a 10-fold
223 increase of sfRNA1 and 400-fold increase of sfRNA2 relative to gRNA, confirming the
224 presence and high abundance of the two sfRNAs during KRV infection. Finally, we
225 characterized the 5' start site of the subgenomic RNA species using a 5'-3' ligation assay.
226 This analysis confirmed that sfRNA1 and sfRNA2 started immediately upstream of xrRNA1
227 and xrRNA2, resulting in products of 1017 nt and 421-422 nt, respectively (Fig. 3E).

228

229 With the new characterization of the KRV sfRNAs, we further analyzed our small RNA
230 sequencing data (Fig. 1–2) and investigated the vsiRNA distribution on the genomic region

231 corresponding to the sfRNA downstream from the xrRNA structures, either expressed as a
232 percentage of the genome-mapping vsiRNAs (Fig. 4A) or as a density of vsiRNA reads per nt
233 (Fig. 4B). The sfRNA region of CFAV, which covers 92% of its 3'UTR (Fig. 3B), was
234 clearly associated with a higher density of vsiRNAs. In contrast, only a negligible amount of
235 KRV vsiRNA derived from its gRNA-specific regions (<7%), whereas 92% of KRV vsiRNA
236 mapped to the sfRNA region in the 3' UTR. Thus, the 3' bias characteristic of cISF and
237 especially KRV-derived vsiRNAs correlated highly with the sfRNA region of the 3'UTR.

238

239 **Biogenesis of KRV sfRNA is Pacman-dependent**

240 To determine whether sfRNA biogenesis is *Pacman*-dependent, we used CRISPR/Cas9 gene
241 editing to create *Pacman* knockout (KO) U4.4 cell lines. Several putative *Pacman* loci are
242 annotated in the *Ae. albopictus* genome, of which AALFPA_065179, AALFPA_057530 and
243 AALFPA_079140 contain the conserved 5'-3' exoribonuclease domain (> 98% identity
244 across loci), whereas AALFPA_052256 only contains the SH3-like domain and is unlikely to
245 encode a functional Pacman nuclease (Fig. S3A). Guide RNAs were designed to introduce
246 frameshift mutations leading to premature stop codons in the 5'-3' exoribonuclease domain.
247 Two *Pacman* KO U4.4 cell clones were obtained (g3#3 and g2#13), which were compared to
248 a CRISPR control line (CTRL) that was subjected in parallel to the same treatment without
249 functional guide RNA, and to the wildtype (WT) parental U4.4 cell line. *Pacman* mRNAs
250 containing the 5'-3' exoribonuclease domain were unstable in both *Pacman* KO U4.4 cell
251 clones (Fig. S3B), likely due to nonsense mediated decay induced by the presence of
252 premature stop codons. KRV replicated to similar levels in *Pacman* KO cells as in WT and
253 CTRL cells (Fig. S3C).

254 Using northern blotting, we observed lower levels of sfRNA1 and sfRNA2 in KRV infected
255 *Pacman* KO cells, confirming that their biogenesis is *Pacman*-dependent (Fig. 5A).

256 Interestingly, two different ~800 nt and ~500 nt subgenomic RNAs were identified in
257 *Pacman* KO cells, which we named sfRNA1' and sfRNA2', likely the products of redundant
258 5'-3' exoribonucleases stalling on structures downstream of xrRNA1 (63, 64). This is
259 reminiscent of the appearance of other RNA species without loss of sfRNA upon knockdown
260 of XRN1 in human cells (65). Processing of viral RNA by other 5'-3' exoribonucleases
261 would also explain why viral gRNA was not stabilized in *Pacman* KO cells (Fig. 5A, Fig.
262 S3C)

263 The exact 5' start sites of sfRNA1' and sfRNA2' were determined by 5'-3'end ligation to be
264 at nt 10,533 (9/9 clones) and 10,830 (4/5 clones) of the KRV genome, respectively. These
265 sites did not correspond to notable predicted structures or RNA motifs (Fig. 3B, data not
266 shown). Overall, the production of KRV sfRNA is *Pacman*-dependent and its absence leads
267 to the production of alternative sfRNAs shorter than sfRNA1.

268

269 **Viral small RNA production in *Pacman* knockout cells**

270 In absence of an infectious clone required to generate KRV without sfRNA and study its role
271 in siRNA production, we took advantage of the shift in sfRNA production in *Pacman* KO
272 cells as a substitute to investigate putative sfRNA-derived siRNAs. We explored the
273 involvement of sfRNAs in the 3' bias of KRV vsiRNAs by comparing vsiRNA profiles in
274 U4.4 CTRL cells with *Pacman* KO cells, in which two new KRV subgenomic RNAs were
275 produced (sfRNA1' and 2'; Fig. 5A).

276 Interestingly, total siRNA levels were higher in *Pacman* KO cells than in control cells (Fig.
277 5B), perhaps due to the higher processing of mRNA by the siRNA pathway when the RNA
278 decay pathway was impaired. In contrast, vsiRNA levels decreased slightly for KRV and
279 ZIKV in the absence of Pacman (Fig. 5C, S3C). Surprisingly, in the segment differentiating
280 KRV sfRNA1 from the *Pacman* KO associated sfRNA1' and 2' (nt 10361-10533), no

281 difference in vsiRNA distribution was observed (Fig. 5D, 5F). Similarly, no major
282 differences were observed for vsiRNA profiles of ZIKV between *Pacman* KO and CTRL
283 cells (Fig. 5E, 5G). Further, presentation of the KRV vsiRNA on a logarithmic scale indicates
284 that the 3'bias in starting upstream of the 3'UTR, around positions 9890-10010, in a *Pacman*-
285 independent manner (Fig. 1B, 5I). These results demonstrate that while KRV 3' biased
286 vsiRNAs correlate strongly with the 3'UTR and by extension its sfRNA region, they are not
287 produced from sfRNA species.

288 DISCUSSION

289 Within the *Flavivirus* genus, cISFs constitute a unique clade of viruses that evolved
290 independently, only infecting invertebrate hosts in which they are not associated with known
291 disease (66). As such, cISFs represent a prime resource to better understand viral infection
292 and antiviral immunity in mosquitoes. In a pan-flavivirus small RNA analysis, we found that
293 vsiRNAs generally mapped across the viral genome for most mosquito-specific and
294 mosquito-borne viruses, while there was a strong vsiRNA bias toward the 3' UTR of KRV,
295 the production of which was independent of its two, highly abundant sfRNAs.

296

297 **Unique RNAi response toward classical insect specific flaviviruses is sfRNA-
298 independent**

299 RNAi is a cornerstone of mosquito immunity comparable to the importance of the interferon
300 response in mammalian systems, as its deficiency leads to increased sensitivity to viral
301 infections (36, 67–69). Our analysis strengthens previous observations in *Anopheles* (70),
302 *Culex* (55, 71) and *Aedes* (45, 67) that mosquito RNAi raises a broad and uniform antiviral
303 response against all assessed mosquito-borne flaviviruses. Yet, cISFs seem to have evolved
304 to produce a unique RNAi response with vsiRNAs biased towards the 3' UTR of the viral
305 genome, which was particularly strong for KRV but also detectable for CxFV, CFAV, and
306 previously for AEFV (3). Interestingly, we did not observe a 3' vsiRNA bias for the dISF
307 NOUV, indicating that the biased vsiRNA production is not required for a mosquito-
308 restricted transmission cycle.

309 The homogeneous distribution across the genome and the absence of a strand bias of
310 vsiRNAs is consistent with processing of flaviviruses dsRNA consisting of (+) and (-) gRNA
311 hybrids (36). The 3' vsiRNA bias of KRV and other cISFs suggest a correlation with viral
312 RNA species produced specifically by cISFs, which remain to be elucidated. A 3' vsiRNA

313 bias has previously been suggested to be related to sfRNA and RNA structure of the region
314 (3), but our data do not support such hypothesis. First, KRV vsiRNAs derive equally from
315 sfRNA1 or sfRNA2 regions, while more vsiRNAs would be expected toward the 3' end due
316 to the high abundance of both sfRNA1 and sfRNA2 (23, 28, 31). Second, a shift in sfRNA
317 production is observed in *Pacman*-knockout cells, but this did not affect vsiRNA patterns.
318 Third, (+) and (-) sense vsiRNAs are present at roughly equimolar levels, whereas sfRNA is a
319 (+) sense RNA, which would result in a strong (+) strand bias of siRNAs should sfRNA be
320 the Dicer-2 substrate. Fourth, the vsiRNA 3' bias starts upstream of the 3' UTR and the
321 sfRNAs. Thus, the mechanism underlying the 3' bias of vsiRNAs remains to be understood
322 and may be multi-factorial. It was proposed that sfRNAs could bind the 5' end of (-) gRNA
323 as a competitive regulator of RNA replication (72–74), which would generate a double-
324 stranded Dicer substrate, but this is not be consistent with our observations and arguments as
325 outlined above, and would not account for a significant fraction of 3'UTR derived vsiRNAs.
326 Therefore, previous suggestions that cISF 3' biased siRNAs can be attributed to the sfRNA
327 (3, 50, 57) are likely due to the sfRNA region covering most of the 3'UTR and a more
328 moderate 3' UTR biased siRNA profile that does not allow enough resolution. Instead, our
329 data suggest the presence of an as yet unknown subgenomic dsRNA species of approximately
330 1500 nt that is colinear with the 3' end of the viral genome. Effective processing of such a
331 dsRNA molecule by the RNAi machinery may explain that it has escaped detection in our
332 northern blot analyses.

333

334 Conclusion

335 As part of the constant arms race between viruses and their hosts (75), cISFs and especially
336 KRV seem to have evolved unique ways to maintain themselves in mosquito populations.
337 KRV's strikingly long 3' UTR representing 10% of its total gRNA, combined with the

338 expression of two highly abundant sfRNAs, as well as the strong 3' bias of vsiRNAs makes
339 KRV an intriguing model to study the biology of cISFs and the mechanisms of mosquito
340 antiviral immunity.

341

342 ACKNOWLEDGEMENTS

343 We thank Pascal Miesen for preliminary analysis of small RNA sequencing data. We thank
344 Andrea Gamarnik (Fundación Instituto Leloir, Buenos Aires, Argentina) for advice on the 5'-
345 3' ligation method. We thank Beate Kümmerer (University of Bonn) for providing DENV2
346 strain 16681 and M. Niedrig (Robert-Koch-Institute, Berlin) for providing WNV strain NY-
347 99. CFAV (isolate Rio Piedras), CxFV (isolate Uganda08), KRV (isolate SR-75) and ZIKV
348 (isolate H/PF/2013) were provided by Xavier de Lamballerie (Aix Marseille Université)
349 through the European Virus Archive (EVAg), funded by the European Union's Horizon 2020
350 programme. This study was financially supported by the Deutsche Forschungsgemeinschaft
351 (DFG) within Priority Programme SPP1596 [grant number JU 2857/1-1 and JU2857/1-2 to
352 SJ and grant number VA 827/1-1 and RI 2381/1-2 to RPvR] and by a European Research
353 Council Consolidator Grant under the European Union's Seventh Framework Programme
354 [grant number ERC CoG 615680 to RPvR]. Small RNA sequencing was performed by the
355 GenomEast platform, a member of the “France Génomique” consortium (ANR-10-INBS-
356 0009).

357 MATERIAL AND METHODS

358 **Cells and viruses**

359 *Aedes albopictus* C6/36 cells (ECACC General Cell Collection, #89051705) and U4.4 cells
360 (kindly provided by G.P. Pijlman, Wageningen University, the Netherlands) were cultured at
361 28°C in Leibovitz L15 medium (Gibco) supplemented with 10% heat inactivated fetal calf
362 serum (Sigma), 2% tryptose phosphate broth solution (Sigma), 1x MEM non-essential amino
363 acids (Gibco), and 50 U/ml penicillin and 50 µg/ml streptomycin (Gibco).
364 CFAV (isolate Rio Piedras), CxFV (isolate Uganda08), KRV (isolate SR-75) and ZIKV
365 (isolate H/PF/2013) were obtained from the European Virus Archive. DENV2 (strain 16681)
366 was provided by Beate Kümmeler, University of Bonn. SLEV (strain MSI-7) was obtained
367 from the National Collection of Pathogenic Viruses, Porton Down, Salisbury, United
368 Kingdom and WNV (strain NY-99) was kindly provided by M. Niedrig, Robert-Koch-
369 Institute, Berlin, Germany. SLEV (Palenque) and NOUV (isolate B3) were previously
370 characterized (54, 76). Reference sequences are listed in Table S1.

371

372 **Plasmids**

373 Plasmids used as standard to normalize the qPCR data were obtained by blunt end ligation of
374 the flavivirus qPCR products into pGEM-3Z (Promega), using SmaI (NEB) and T4 DNA
375 ligase (Roche). For KRV RNA species quantification, plasmid pUC57-KRV-9000-11375
376 containing part of NS5 gene and the 3' UTR of KRV (nt 9000-11375) was synthesized by
377 GenScript.

378 The pAc-Cas9-AalbU6.2 plasmid was generated by replacing the *D. melanogaster* *U6*
379 promoter in the pAc-sgRNA-Cas9 (kindly provided by Ji-Long Liu, Addgene plasmid
380 #49330) (77) with the *Ae. albopictus* promoter from AALFPA_045636 and by introducing
381 XbaI restriction sites using In-Fusion cloning (Takara) on four fragments amplified using the

382 primers in Table S2, according to the manufacturer's instructions. sgRNA sequences
383 targeting *Pacman* were cloned into a SapI restriction site directly downstream of the U6
384 promoter by annealing and phosphorylating complementary oligonucleotides (Table S2),
385 followed by ligation using T4 DNA ligase (Roche), replacing the 5'-
386 GGAAGAGCGAGCTCTTCC-3' sequence that was used as negative control for
387 CRISPR/Cas9 knockouts.

388

389 **CRISPR/Cas9**

390 U4.4 cells were transfected with the pAc-Cas9-AalbU6.2 plasmid, which expresses 3xFLAG-
391 tagged Cas9 with N- and C-terminal SV40 nuclear localization signals, followed by a viral
392 2A ribosome self-cleavage site and the puromycin N-acetyltransferase coding sequence,
393 driven by the *D. melanogaster Actin5c* promoter. In parallel to the plasmid encoding *Pacman*
394 sgRNA, cells were transfected with the parental pAc-Cas9-AalbU6.2 plasmid to generate the
395 CRISPR control (CTRL) cells. U4.4 cells were seeded in a 24-well plate and transfected the
396 next day with 500 ng of plasmid, using X-tremeGENE HP transfection reagent (Roche)
397 according to the manufacturer's instructions. At 2 days after transfection, puromycin
398 (InvivoGen) was added to the culture medium at a concentration of 20 µg/ml and 4 days
399 later, the cells were transferred to a new plate at a 1:2 dilution, in medium containing 20
400 µg/ml puromycin. The other half of the cells was used for genomic DNA isolation (Zymo
401 Research #D3024) and PCR (Promega #M7806) using primers flanking the sequence targeted
402 by the sgRNA (Table S2) to assess editing efficiency. Multiple sgRNA constructs were
403 initially constructed and the constructs with the highest editing efficiency were selected,
404 assessed by size heterogeneity of the PCR products on ethidium bromide-stained agarose gel.
405 Cells transfected with these sgRNA constructs (g2 and g3) were seeded in 96-well plates at a
406 density of a single cell per well in supplemented L15 medium in the absence of puromycin.

407 After 3 weeks, gDNA was isolated from the single-cell clones, followed by PCR and Sanger
408 sequencing of the targeted *Pacman* locus. Based on the sequencing results U4.4 clones g2#13
409 and g3#3, both containing only out-of-frame deletions in the *Pacman* coding region, were
410 selected for further analyses.

411

412 **Small RNA library preparation and analysis**

413 U4.4 cells were seeded at a density of 2×10^6 cells per well in 6-well plates and infected the
414 following day with the designated flaviviruses at an MOI of 0.1. Cells were harvested at 72
415 hours post infection (hpi) in RNA-Solv reagent (Omega Bioteck R630-02) for total RNA
416 isolation. 1 μ g of RNA was used as input for library preparation using the NEBNext
417 Multiplex Small RNA Library Prep Kit for Illumina (NEB E7560S), according to the
418 manufacturer's recommendations. The libraries were size-selected on 6% polyacrylamide/1x
419 TBE gels, quantified using the Agilent 2100 Bioanalyzer System, and pooled for sequencing
420 on an Illumina HiSeq4000 machine by the GenomEast Platform (Strasbourg, France). Viral
421 small RNA sequences were mapped to the designated genome (Table S1) using Bowtie
422 (Galaxy Tool Version 1.1.2) (78) allowing 1 mismatch. The genome distribution of the viral
423 small RNAs was obtained by plotting the 5' ends of mapping reads on the viral genome
424 sequence. Nucleotide biases were plotted using the WebLogo 3 program (Galaxy Tool
425 Version 0.4). All reads were normalized by library size as reads per million. The small RNA
426 sequencing datasets have been deposited at the Sequence Read Archive under accession
427 number PRJNA830662.

428

429 **Reverse transcription and quantitative PCR**

430 For RT-qPCR, 1 μ g of total RNA was reverse transcribed in a 20 μ l reaction using Taqman
431 RT Reagents (ThermoFisher Scientific) with hexamers at 48°C for quantification of viral

432 RNA copies or SuperScript IV Reverse Transcriptase (ThermoFisher Scientific) with primer
433 5'-AGCGCATTATGGTATAGAAAAAGA-3' at 60°C for quantification of specific KRV
434 RNA species. Quantitative PCR was performed using the GoTaq qPCR SYBR mastermix
435 (Promega) on a LightCycler 480 instrument (Roche). A standard curve of plasmids
436 containing the corresponding viral sequence was used to convert Ct values to relative viral
437 RNA copy numbers. *Pacman* mRNA levels were normalized to house-keeping gene
438 *ribosomal protein L5*. For qPCR primer sequences, see Table S2.

439

440 Northern Blot

441 5 µg of total RNA was separated on a 1X MOPS, 5% formaldehyde, 0.8% agarose gel for 5
442 h, transferred on a Hybond NX nylon membrane (Amersham) and cross-linked in the Gene
443 linker UV chamber (Bio-Rad). Viral RNAs were detected with DNA oligonucleotides (Table
444 S2) end-labelled with [³²P] γ-adenosine-triphosphate (Perkin Elmer) using T4 polynucleotide
445 kinase (Roche). Hybridization to the oligonucleotide probes was performed overnight at 42°C
446 in Ultra-hyb Oligo hybridization buffer (Ambion). Membranes were then washed three times
447 at 42°C with decreasing concentrations of SDS (0.2 to 0.1%) and exposed to X-ray films
448 (Carestream).

449

450 5' to 3' end ligation

451 The 5' ends of KRV RNA species were determined by 5' to 3' end ligation using a method
452 adapted from (11, 79). C6/36 cells were seeded at a density of 4x10⁶ cells per T75 flask and
453 infected the following day with KRV at an MOI of 10. Cells were harvested at 48 hpi and
454 RNA was isolated using RNA-Solv reagent and 10 µg of total RNA was treated with T4
455 RNA ligase (Epicenter). Ligated RNAs were reverse transcribed with Taqman Multiscribe
456 (Applied Biosystem) using random hexamers. The 5'-3' junction region was amplified by

457 PCR using a forward primer at the end of the 3' UTR and a reverse primer in the 5' part of
458 KRV RNA species (Table S2), cloned into pGEM-3Z (Promega) using In-Fusion technology
459 (Takara) and Sanger sequenced by the in-house sequencing facility.

460

461 **RNA structure prediction and bioinformatics**

462 RNA secondary structure were predicted in the 3'UTR regions of KRV, CFAV, CxFV, and
463 XFV using the ViennaRNA Package v.2.5.1 (80). Evolutionarily conserved elements were
464 identified with the help of the viRNA GitHub repository (<https://github.com/mtw/viRNA>),
465 and used as constraints for RNA structure prediction. Locally stable RNA structures were
466 predicted with RNALfold from the ViennaRNA Package, allowing for a maximal base pair
467 span of 100 nt.

468 Multiple sequence alignments of whole genome and 3' UTR sequences were generated with
469 MAFFT (81), curated with BMGE (82) and a maximum likelihood phylogenetic tree was
470 built with PhyML (83) using NGPhylogeny.fr (84) using default settings. Phylogenetic trees
471 were visualized on iTOL (85). Percentage identities were determined with Mview (86).

472 Viral reference sequences are listed in Table S3.

473

474 **Statistical analysis**

475 Graphical representation and statistical analyses were performed using GraphPad Prism v7
476 software. Differences were tested for statistical significance using one- or two-way ANOVA
477 and Fisher's LSD test.

478

479 LEGENDS

480 **Figure 1. Comparison of flavivirus-derived small RNAs in U4.4 cells**

481 (A) Maximum likelihood phylogenetic tree based on whole genome sequences of the indicated
482 viruses. Branch lengths are proportional to the number of substitutions per site. MBF,
483 mosquito-borne flavivirus; ISF, insect-specific flavivirus. (B) Size profiles of flavivirus-
484 derived small RNAs in read per million (RPM) from U4.4 cells infected for 72 h at an MOI
485 of 0.1. Positive-sense RNAs are shown in red, negative-sense RNA in blue. Ratios of viral
486 piRNAs over siRNAs are indicated for each virus. The results are the average of two
487 experiments for all flaviviruses, except for CxFV (n = 1), CFAV (n = 3, of which 2 in WT
488 U4.4 cells and 1 in CRISPR CTRL U4.4 cells), and KRV (n = 3). Error bars are the standard
489 deviation between replicates.

490

491

492 **Figure 2. KRV vsiRNAs are strongly biased towards the 3' UTR**

493 (A) Distribution of flavivirus-derived vsiRNAs across the genome of each virus in reads per
494 million (RPM) from U4.4 cells infected at a MOI of 0.1 for 72h. Start and end of the 3' UTRs
495 are indicated by dashed vertical lines. (B) Distribution of KRV vsiRNAs on a logarithmic
496 scale with the position of the 3' UTR indicated. (C) Percentage of vsiRNAs mapping to the
497 3' UTR compared to the whole genome sequence for the indicated flaviviruses. The dashed
498 horizontal line indicates the median of 3' UTR derived vsiRNA from non-cISFs. (A-C) The
499 results are the average of two experiments for all flaviviruses, except for CxFV (n = 1) and
500 KRV (n = 3). Error bars are the standard deviation between replicates for each individual
501 nucleotide. Positive-strand RNAs are shown in red, negative-strand RNAs in blue. ** p <
502 0.01; by two-way ANOVA and Fisher's LSD test.

503

504

505 **Figure 3. KRV has a long and unique 3' UTR and produces high quantities of sfRNA**

506 **(A)** Length of the 3' UTR of all members of the *Flavivirus* genus with a RefSeq, a complete
507 coding genome and a 3' UTR of at least 200 nt. Viruses belong to the clades indicated: cISF,
508 classical insect specific flaviviruses; dISF, dual-host affiliated insect specific flaviviruses;
509 MBF, mosquito-borne flaviviruses; NKV, no known vector; TBF, tick-borne flaviviruses. For
510 virus name and accession numbers, see Table S1. **(B)** Secondary structure prediction of the
511 3'UTR of four ISFs. Maximum likelihood phylogenetic tree and alignment of 3' UTR of listed
512 viruses with conserved regions as described in (87). Branch lengths are proportional to the
513 number of substitutions per site. Evolutionarily conserved RNA elements are highlighted in
514 colour, with structurally homologous elements in the same colour. Elements without colour
515 represent locally stable RNA structures from single-sequence RNA structure predictions.
516 Exoribonuclease-resistant structures (xrRNA) in KRV, CFAV and AEFV are shown in blue,
517 including reported pseudoknot interactions (17) with sequence regions downstream of the
518 three-way junction structures. Repeat elements a (Ra) and b (Rb) (21) are depicted in olive
519 and orange, respectively. 3' stem-loop elements (3'SL) are shown in dark green. The internal
520 3'SL element of KRV is predicted to adopt a longer closing stem, which lacks evolutionary
521 support in other viruses. The same applies for the extended closing stems of Ra elements in
522 XFV. Percent nucleotide identities of each virus to KRV are indicated for the region between
523 xrRNA2 and the 3' SL. Lengths of the 3' UTRs are indicated on the right. **(C)** Northern blot
524 of positive-sense viral RNA in U4.4 cells infected with either NOUV or KRV at an MOI of
525 0.1 or mock infected for 72 h. Viral RNA was detected using a pool of oligonucleotide
526 probes complementary to the 3' UTR of KRV, between positions 10,361 and 11,375. All
527 images were captured from the same northern blot. **(D)** Relative RT-qPCR quantification of
528 KRV RNA in U4.4 cells infected for 72 h at an MOI of 0.1. Data are expressed relative to

529 gRNA copy numbers and bars indicate means and standard deviation of four replicates. * $p <$
530 0.05; ** $p < 0.01$ by one-Way ANOVA and Fisher's LSD test. (E) Position of 5' ends of
531 KRV sfRNA1 and sfRNA2 defined by 5' to 3' end ligation and sequencing, displayed on the
532 consensus xrRNA structure predicted from SHAPE data for CFAV xrRNA1, which is 90%
533 identical to KRV xrRNA1 and xrRNA2 (59).

534

535 **Figure 4. cISF-derived siRNA correlate with the sfRNA region of their genome**

536 (A) Percentage of vsiRNAs compared to the whole genome sequence and (B) average density
537 of vsiRNAs per nucleotide in the indicated regions of the genome of CFAV (left) or KRV
538 (right). The size of each region is indicated in italic as a percentage of the genome size. (A–
539 B) The results are the average of two experiments for all flaviviruses, except for CxFV ($n =$
540 1) and KRV ($n = 3$). Error bars are the standard deviation between replicates for each
541 individual nucleotide. Positive-strand RNAs are shown in red, negative-strand RNAs in blue.
542 ** $p < 0.01$; **** $p < 0.0001$ by two-way ANOVA and Fisher's LSD test.

543

544

545 **Figure 5. Pacman knockout does not affect vsiRNA profiles**

546 (A) Northern blot of positive-sense (+) RNA or negative-sense (-) RNA viral RNA in
547 control (CTRL) cells or *Pacman* knockout cells (clones g3#3 and g2#13), mock infected (-)
548 or infected with KRV (+) at an MOI of 0.1 for 72 h. Viral RNA was detected using a pool of
549 oligonucleotide probes complementary to the 3' UTR of KRV, between positions 10,361 and
550 11,375. The location of ribosomal RNA (rRNA) based on ethidium bromide staining is
551 indicated. (B–C) Quantification of total siRNAs (B) and sense (+) and antisense (-) vsiRNAs
552 (C) in wild-type (WT), CRISPR control (CTRL), or *Pacman* knockout (KO) U4.4 cell lines
553 infected with ZIKV at an MOI of 0.1 or KRV at an MOI of 10 for 72 h. Viral siRNA levels

554 were normalized to viral gRNA levels. Errors bars represent the standard deviation from two
555 independent cell lines. ns, non-significant; *, $p < 0.05$ by two-way ANOVA and Fisher's
556 LSD test. **(D-E)** Distribution of (+) and (-) vsiRNAs across the 3' end of the genomes of
557 KRV (**D**) or ZIKV (**E**) (from nt 9000 onwards) in CTRL and *Pacman* KO cells. Top panels
558 show (+) vsiRNAs and lower panels show (-) vsiRNAs. The results are the average from two
559 independent cell lines. **(F-G)** Percentage of vsiRNAs derived from the indicated regions
560 compared to the entire gRNA. The size of each region is indicated in *italic* as a percentage of
561 the viral genome size. Errors bars represent the standard deviation from two independent cell
562 lines. **(I)** Distribution of KRV vsiRNAs on a logarithmic scale plotted on the 3' terminal
563 region of the genome. **(D-E, I)** Boundaries of 3' UTRs and sfRNAs are indicated by dashed
564 vertical lines. **(D-G)** Blue, (+) vsiRNA; red, (-) vsiRNA; darker, WT and CTRL cells; lighter,
565 *Pacman*-KO cells.

566

567 **Supplementary figure 1. Relative quantification of gRNA, vsiRNA and vpiRNA.**

568 **(A)** Quantification of viral gRNA copies, **(B)** total vsiRNA over gRNA copy ratios, and **(C)**
569 (+) vpiRNA over gRNA copy ratios in the samples analyzed in Figures 1–2 and S2. U4.4
570 cells were infected with the indicated virus at a MOI of 0.1 for 72h. Error bars are the
571 standard deviation of at least 2 independent experiments. ns, non-significant by one-way
572 ANOVA and Fisher's LSD test.

573

574 **Supplementary figure 2. Viral piRNA profiles of flavivirus infected U4.4 cells**

575 Distribution of flavivirus derived 25–30 nt vpiRNAs on the genome of each virus in reads per
576 million (RPM) from U4.4 cells infected for 72h at a MOI of 0.1. In boxes, sequence logos at
577 position 1 and 10 of 25–30 nt vpiRNAs. The results are the average of two experiments for

578 all flaviviruses, except for CxFV (n=1) and KRV (n=3). Error bars are the standard deviation
579 between replicates. Positive-strand RNAs are shown in red, negative-strand RNA in blue.

580

581 **Supplementary figure 3. Characterization of flavivirus infection of *Pacman*-KO U4.4**
582 **cells**

583 (A) *Pacman* KO U4.4 cell lines were generated by CRISPR/Cas9 technology, amplified from
584 single clones, and the edited sites in exon 4 were Sanger sequenced. Sequencing identified
585 three small deletions that all induced out-of-frame mutations in the exoribonuclease domain
586 in both *Pacman* KO clones. Gene structure, conserved domains, and primer sets used in (B)
587 are indicated. (B) Relative quantification by RT-qPCR of *Pacman* mRNA in CTRL and
588 *Pacman* KO cells infected with KRV at a MOI of 1 for 96h. *Pacman* mRNA levels were
589 normalized to house-keeping gene *ribosomal protein L5* and expressed relative to *Pacman*
590 mRNA levels in WT cells. (C) Quantification of ZIKV or KRV RNA in cells and culture
591 supernatants of the indicated U4.4 cells at 72 h post infection at an MOI of 0.1 or 10.

592

593 **Supplementary table 1. List of viruses used**

594

595 **Supplementary table 2. List of oligonucleotides for northern blots, qPCR and cloning**

596

597 **Supplementary table 3. List of genome references used for 3'UTR analysis**

598

599 REFERENCES

- 600 1. Postler TS, Beer M, Blitvich BJ, Bukh J, de Lamballerie X, Drexler JF, Imrie A, Kapoor
601 A, Karganova GG, Lemey P, Lohmann V, Simmonds P, Smith DB, Stapleton JT, Kuhn
602 JH. 2023. Renaming of the genus Flavivirus to Orthoflavivirus and extension of
603 binomial species names within the family Flaviviridae. *Arch Virol* 168:224.
- 604 2. Saiyasombat R, Bolling BG, Brault AC, Bartholomay LC, Blitvich BJ. 2011. Evidence of
605 Efficient Transovarial Transmission of Culex Flavivirus by Culex pipiens (Diptera:
606 Culicidae). *J Med Entomol* 48:1031–1038.
- 607 3. Frangeul L, Blanc H, Saleh M-C, Suzuki Y. 2020. Differential Small RNA Responses
608 against Co-Infecting Insect-Specific Viruses in Aedes albopictus Mosquitoes. *Viruses*
609 12:468.
- 610 4. Blitvich B, Firth A. 2015. Insect-Specific Flaviviruses: A Systematic Review of Their
611 Discovery, Host Range, Mode of Transmission, Superinfection Exclusion Potential
612 and Genomic Organization. *Viruses* 7:1927–1959.
- 613 5. Moureau G, Cook S, Lemey P, Nougairède A, Forrester NL, Khasnatinov M, Charrel
614 RN, Firth AE, Gould EA, de Lamballerie X. 2015. New Insights into Flavivirus
615 Evolution, Taxonomy and Biogeographic History, Extended by Analysis of Canonical
616 and Alternative Coding Sequences. *PLoS One* 10:e0117849–30.
- 617 6. Hall RA, Bielefeldt-Ohmann H, McLean BJ, O'Brien CA, Colmant AMG, Piyasena
618 TBH, Harrison JJ, Newton ND, Barnard RT, Prow NA, Deerain JM, Mah MGKY,
619 Hobson-Peters J. 2016. Commensal Viruses of Mosquitoes: Host Restriction,
620 Transmission, and Interaction with Arboviral Pathogens. *Evolutionary Bioinformatics*
621 12S2:EBO.S40740.
- 622 7. Pierson TC, Diamond MS. 2020. The continued threat of emerging flaviviruses. *Nat
623 Microbiol* 5:796–812.
- 624 8. Porier DL, Wilson SN, Auguste DI, Leber A, Coutermash-Ott S, Allen IC, Caswell CC,
625 Budnick JA, Bassaganya-Riera J, Hontecillas R, Weger-Lucarelli J, Weaver SC,
626 Auguste AJ. 2021. Enemy of My Enemy: A Novel Insect-Specific Flavivirus Offers a
627 Promising Platform for a Zika Virus Vaccine. *Vaccines (Basel)* 9:1142.
- 628 9. Hobson-Peters J, Harrison JJ, Watterson D, Hazlewood JE, Vet LJ, Newton ND,
629 Warrilow D, Colmant AMG, Taylor C, Huang B, Piyasena TBH, Chow WK, Setoh YX,
630 Tang B, Nakayama E, Yan K, Amarilla AA, Wheatley S, Moore PR, Finger M, Kurucz
631 N, Modhiran N, Young PR, Khromykh AA, Bielefeldt-Ohmann H, Suhrbier A, Hall RA.
632 2019. A recombinant platform for flavivirus vaccines and diagnostics using chimeras
633 of a new insect-specific virus. *Sci Transl Med* 11.
- 634 10. Vet LJ, Setoh YX, Amarilla AA, Habarugira G, Suen WW, Newton ND, Harrison JJ,
635 Hobson-Peters J, Hall RA, Bielefeldt-Ohmann H. 2020. Protective Efficacy of a
636 Chimeric Insect-Specific Flavivirus Vaccine against West Nile Virus. *Vaccines (Basel)*
637 8:258.
- 638 11. Varjak M, Donald CL, Mottram TJ, Sreenu VB, Merits A, Maringer K, Schnettler E,
639 Kohl A. 2017. Characterization of the Zika virus induced small RNA response in Aedes
640 aegypti cells. *PLoS Negl Trop Dis* 11:e0006010.
- 641 12. De Falco L, Silva NM, Santos NC, Huber RG, Martins IC. 2021. The Pseudo-Circular
642 Genomes of Flaviviruses: Structures, Mechanisms, and Functions of Circularization.
643 *Cells* 10:642.

- 644 13. Mazeaud C, Freppel W, Chatel-Chaix L. 2018. The Multiples Fates of the Flavivirus
645 RNA Genome During Pathogenesis. *Front Genet* 9.
- 646 14. Fajardo T, Sanford TJ, Mears H V., Jasper A, Storrie S, Mansur DS, Sweeney TR.
647 2020. The flavivirus polymerase NS5 regulates translation of viral genomic RNA.
648 *Nucleic Acids Res* 48:5081–5093.
- 649 15. Trettin KD, Sinha NK, Eckert DM, Apple SE, Bass BL. 2017. Loquacious-PD facilitates
650 Drosophila Dicer-2 cleavage through interactions with the helicase domain and
651 dsRNA. *Proceedings of the National Academy of Sciences* 114:E7939–E7948.
- 652 16. Pijlman GP, Funk A, Kondratieva N, Leung J, Torres S, van der Aa L, Liu WJ,
653 Palmenberg AC, Shi PY, Hall RA, Khromykh AA. 2008. A Highly Structured,
654 Nuclease-Resistant, Noncoding RNA Produced by Flaviruses Is Required for
655 Pathogenicity. *Cell Host Microbe* 4:579–591.
- 656 17. MacFadden A, O'Donoghue Z, Silva PAGCGC, Chapman EG, Olsthoorn RC, Sterken
657 MG, Pijlman GP, Bredenbeek PJ, Kieft JS. 2018. Mechanism and structural diversity
658 of exoribonuclease-resistant RNA structures in flaviviral RNAs. *Nat Commun* 9:119.
- 659 18. Slonchak A, Khromykh AA. 2018. Subgenomic flaviviral RNAs: What do we know
660 after the first decade of research. *Antiviral Res*
661 <https://doi.org/10.1016/j.antiviral.2018.09.006>.
- 662 19. Vicens Q, Kieft JS. 2021. Shared properties and singularities of exoribonuclease-
663 resistant RNAs in viruses. *Comput Struct Biotechnol J* 19:4373–4380.
- 664 20. Kieft JS, Rabe JL, Chapman EG. 2015. New hypotheses derived from the structure of
665 a flaviviral Xrn1-resistant RNA: Conservation, folding, and host adaptation. *RNA Biol*
666 12:1169–1177.
- 667 21. Ochsenreiter R, Hofacker I, Wolfinger M. 2019. Functional RNA Structures in the
668 3' UTR of Tick-Borne, Insect-Specific and No-Known-Vector Flaviruses. *Viruses*
669 11:298.
- 670 22. Villordo SM, Filomatori C V, Sánchez-Vargas I, Blair CD, Gamarnik A V. 2015. Dengue
671 Virus RNA Structure Specialization Facilitates Host Adaptation. *PLoS Pathog*
672 11:e1004604--22.
- 673 23. Filomatori C V., Carballeda JM, Villordo SM, Aguirre S, Pallarés HM, Maestre AM,
674 Sánchez-Vargas I, Blair CD, Fabri C, Morales MA, Fernandez-Sesma A, Gamarnik A V.
675 2017. Dengue virus genomic variation associated with mosquito adaptation defines
676 the pattern of viral non-coding RNAs and fitness in human cells. *PLoS Pathog*
677 13:e1006265.
- 678 24. Funk A, Truong K, Nagasaki T, Torres S, Floden N, Balmori Melian E, Edmonds J,
679 Dong H, Shi PY, Khromykh AA. 2010. RNA structures required for production of
680 subgenomic flavivirus RNA. *J Virol* 84:11407–11417.
- 681 25. Pallarés HM, Costa Navarro GS, Villordo SM, Merwaiss F, de Borba L, Gonzalez
682 Lopez Ledesma MM, Ojeda DS, Henrion-Lacritick A, Morales MA, Fabri C, Saleh MC,
683 Gamarnik A V. 2020. Zika Virus Subgenomic Flavivirus RNA Generation Requires
684 Cooperativity between Duplicated RNA Structures That Are Essential for Productive
685 Infection in Human Cells. *J Virol* 94.
- 686 26. Yeh S-C, Tan W-L, Chowdhury A, Chuo V, Kini RM, Pompon J, Garcia-Blanco MA.
687 2021. The anti-immune dengue subgenomic flaviviral RNA is found in vesicles in
688 mosquito saliva 2 and associated with increased infectivity. *bioRxiv*
689 <https://doi.org/10.1101/2021.03.02.433543>.

- 690 27. Moon SL, Anderson JR, Kumagai Y, Wilusz CJ, Akira S, Khromykh AA, Wilusz J. 2012.
691 A noncoding RNA produced by arthropod-borne flaviviruses inhibits the cellular
692 exoribonuclease XRN1 and alters host mRNA stability. *RNA* 18:2029–2040.
693 28. Slonchak A, Hugo LE, Freney ME, Hall-Mendelin S, Amarilla AA, Torres FJ, Setoh YX,
694 Peng NYG, Sng JDJ, Hall RA, van den Hurk AF, Devine GJ, Khromykh AA. 2020. Zika
695 virus noncoding RNA suppresses apoptosis and is required for virus transmission by
696 mosquitoes. *Nat Commun* 11:2205.
697 29. Hussain M, Torres S, Schnettler E, Funk A, Grundhoff A, Pijlman GP, Khromykh AA,
698 Asgari S. 2012. West Nile virus encodes a microRNA-like small RNA in the 3'
699 untranslated region which up-regulates GATA4 mRNA and facilitates virus
700 replication in mosquito cells. *Nucleic Acids Res* 40:2210–2223.
701 30. Pompon J, Manuel M, Ng GK, Wong B, Shan C, Manokaran G, Soto-Acosta R,
702 Bradrick SS, Ooi EE, Missé D, Shi PY, Garcia-Blanco MA. 2017. Dengue subgenomic
703 flaviviral RNA disrupts immunity in mosquito salivary glands to increase virus
704 transmission. *PLoS Pathog* 13:e1006535--27.
705 31. Göertz GP, Fros JJ, Miesen P, Vogels CBF, van der Bent ML, Geertsema C, Koenraadt
706 CJM, van Rij RP, van Oers MM, Pijlman GP. 2016. Noncoding Subgenomic Flavivirus
707 RNA Is Processed by the Mosquito RNA Interference Machinery and Determines
708 West Nile Virus Transmission by *Culex pipiens* Mosquitoes. *J Virol* 90:10145–10159.
709 32. Moon SL, Dodd BJT, Brackney DE, Wilusz CJ, Ebel GD, Wilusz J. 2015. Flavivirus
710 sfRNA suppresses antiviral RNA interference in cultured cells and mosquitoes and
711 directly interacts with the RNAi machinery. *Virology* 485:322–329.
712 33. Phoo WW, Li Y, Zhang Z, Lee MY, Loh YR, Tan YB, Ng EY, Lescar J, Kang C, Luo D.
713 2016. Structure of the NS₂B-NS₃ protease from Zika virus after self-cleavage. *Nat
714 Commun* 1–8.
715 34. Schnettler E, Sterken MG, Leung JY, Metz SW, Geertsema C, Goldbach RW, Vlak JM,
716 Kohl A, Khromykh AA, Pijlman GP. 2012. Noncoding Flavivirus RNA Displays RNA
717 Interference Suppressor Activity in Insect and Mammalian Cells. *J Virol* 86:13486–
718 13500.
719 35. Cirimotich CM, Scott JC, Phillips AT, Geiss BJ, Olson KE. 2009. Suppression of RNA
720 interference increases alphavirus replication and virus-associated mortality in *Aedes
721 aegypti* mosquitoes. *BMC Microbiol* 9:49.
722 36. Bronkhorst AW, van Rij RP. 2014. The long and short of antiviral defense: small RNA-
723 based immunity in insects. *Curr Opin Virol* 7:19–28.
724 37. Marques JT, Imler J-L. 2016. The diversity of insect antiviral immunity: insights from
725 viruses. *Curr Opin Microbiol* 32:71–76.
726 38. Rosendo Machado S, van der Most T, Miesen P. 2021. Genetic determinants of
727 antiviral immunity in dipteran insects – Compiling the experimental evidence. *Dev
728 Comp Immunol* 119:104010.
729 39. Samuel GH, Pohlenz T, Dong Y, Coskun N, Adelman ZN, Dimopoulos G, Myles KM.
730 2023. RNA interference is essential to modulating the pathogenesis of mosquito-
731 borne viruses in the yellow fever mosquito *Aedes aegypti*. *Proceedings of the
732 National Academy of Sciences* 120.
733 40. Dong S, Dimopoulos G. 2023. *Aedes aegypti* Argonaute 2 controls arbovirus
734 infection and host mortality. *Nat Commun* 14:5773.
735 41. Merkling SH, Crist AB, Henrion-Lacritick A, Frangeul L, Couderc E, Gausson V, Blanc
736 H, Bergman A, Baidaliuk A, Romoli O, Saleh M-C, Lambrechts L. 2023. Multifaceted

- 737 contributions of Dicer2 to arbovirus transmission by *Aedes aegypti*. *Cell Rep*
738 42:112977.
- 739 42. Elrefaey AME, Hollinghurst P, Reitmayer CM, Alphey L, Maringer K. 2021. Innate
740 Immune Antagonism of Mosquito-Borne Flaviviruses in Humans and Mosquitoes.
741 *Viruses* 13:2116.
- 742 43. Miesen P, Joosten J, van Rij RP. 2016. PIWIs Go Viral: Arbovirus-Derived piRNAs in
743 Vector Mosquitoes. *PLoS Pathog* 12:e1006017.
- 744 44. Blair CD. 2019. Deducing the Role of Virus Genome-Derived PIWI-Associated RNAs
745 in the Mosquito–Arbovirus Arms Race. *Front Genet* 10.
- 746 45. Miesen P, Ivens A, Buck AH, van Rij RP. 2016. Small RNA Profiling in Dengue Virus 2-
747 Infected *Aedes* Mosquito Cells Reveals Viral piRNAs and Novel Host miRNAs. *PLoS*
748 *Negl Trop Dis* 10:e0004452.
- 749 46. Miesen P, Girardi E, van Rij RP. 2015. Distinct sets of PIWI proteins produce arbovirus
750 and transposon-derived piRNAs in *Aedes aegypti* mosquito cells. *Nucleic Acids Res*
751 43:6545–6556.
- 752 47. Joosten J, Miesen P, Taçsköprü E, Pennings B, Jansen PWTC, Huynen MA,
753 Vermeulen M, van Rij RP. 2019. The Tudor protein Veneno assembles the ping-pong
754 amplification complex that produces viral piRNAs in *Aedes* mosquitoes. *Nucleic
755 Acids Res* 47:2546–2559.
- 756 48. Varjak M, Donald CL, Mottram TJ, Sreenu VB, Merits A, Maringer K, Schnettler E,
757 Kohl A. 2017. Characterization of the Zika virus induced small RNA response in *Aedes
758 aegypti* cells. *PLoS Negl Trop Dis* 11:e0006010.
- 759 49. Tassetto M, Kunitomi M, Whitfield ZJ, Dolan PT, Sánchez-Vargas I, Garcia-Knight M,
760 Ribiero I, Chen T, Olson KE, Andino R. 2019. Control of RNA viruses in mosquito cells
761 through the acquisition of vDNA and endogenous viral elements. *Elife* 8.
- 762 50. Suzuki Y, Baidaliuk A, Miesen P, Frangeul L, Crist AB, Merkling SH, Fontaine A,
763 Lequime S, Moltini-Conclois I, Blanc H, van Rij RP, Lambrechts L, Saleh M-C. 2020.
764 Non-retroviral Endogenous Viral Element Limits Cognate Virus Replication in *Aedes
765 aegypti* Ovaries. *Current Biology* 30:3495–3506.e6.
- 766 51. Palatini U, Miesen P, Carballar-Lejarazu R, Ometto L, Rizzo E, Tu Z, van Rij RP,
767 Bonizzoni M. 2017. Comparative genomics shows that viral integrations are
768 abundant and express piRNAs in the arboviral vectors *Aedes aegypti* and *Aedes
769 albopictus*. *BMC Genomics* 18:512.
- 770 52. Crava CM, Varghese FS, Pischedda E, Halbach R, Palatini U, Marconcini M, Gasmi L,
771 Redmond S, Afrane Y, Ayala D, Paupy C, Carballar-Lejarazu R, Miesen P, Rij RP,
772 Bonizzoni M. 2021. Population genomics in the arboviral vector *Aedes aegypti*
773 reveals the genomic architecture and evolution of endogenous viral elements. *Mol
774 Ecol* 30:1594–1611.
- 775 53. Crabtree MB, Sang RC, Stollar V, Dunster LM, Miller BR. 2003. Genetic and
776 phenotypic characterization of the newly described insect flavivirus, Kamiti River
777 virus. *Arch Virol* 148:1095–1118.
- 778 54. Kopp A, Gillespie TR, Hobelsberger D, Estrada A, Harper JM, Miller RA, Eckerle I,
779 Müller MA, Podsiadlowski L, Leendertz FH, Drosten C, Junglen S. 2013. Provenance
780 and Geographic Spread of St. Louis Encephalitis Virus. *mBio* 4.
- 781 55. Göertz G, Miesen P, Overheul G, van Rij R, van Oers M, Pijlman G. 2019. Mosquito
782 Small RNA Responses to West Nile and Insect-Specific Virus Infections in *Aedes* and
783 *Culex* Mosquito Cells. *Viruses* 11:271.

- 784 56. Saiyasombat R, Bolling BG, Brault AC, Bartholomay LC, Blitvich BJ. 2011. Evidence of
785 Efficient Transovarial Transmission of Culex Flavivirus by Culex pipiens (Diptera:
786 Culicidae). *J Med Entomol* 48:1031–1038.
- 787 57. Rozen-Gagnon K, Gu M, Luna JM, Luo J-D, Yi S, Novack S, Jacobson E, Wang W, Paul
788 MR, Scheel TKH, Carroll T, Rice CM. 2021. Argonaute-CLIP delineates versatile,
789 functional RNAi networks in *Aedes aegypti*, a major vector of human viruses. *Cell Host Microbe* 29:834–848.e13.
- 790 58. Wang Y, Jin B, Liu P, Li J, Chen X, Gu J. 2018. piRNA Profiling of Dengue Virus Type
791 2-Infected Asian Tiger Mosquito and Midgut Tissues. *Viruses* 10:213.
- 792 59. MacFadden A, O'Donoghue Z, Silva PAGC, Chapman EG, Olsthoorn RC, Sterken MG,
793 Pijlman GP, Bredenbeek PJ, Kieft JS. 2018. Mechanism and structural diversity of
794 exoribonuclease-resistant RNA structures in flaviviral RNAs. *Nat Commun* 9:119.
- 795 60. Slonchak A, Parry R, Pullinger B, Sng JDJ, Wang X, Buck TF, Torres FJ, Harrison JJ,
796 Colmant AMG, Hobson-Peters J, Hall RA, Tuplin A, Khromykh AA. 2022. Structural
797 analysis of 3'UTRs in insect flaviviruses reveals novel determinants of sfRNA
798 biogenesis and provides new insights into flavivirus evolution. *Nat Commun* 13:1279.
- 799 61. Göertz GP, van Bree JWM, Hiralal A, Fernhout BM, Steffens C, Boeren S, Visser TM,
800 Vogels CBF, Abbo SR, Fros JJ, Koenraadt CJM, van Oers MM, Pijlman GP. 2019.
801 Subgenomic flavivirus RNA binds the mosquito DEAD/H-box helicase ME31B and
802 determines Zika virus transmission by *Aedes aegypti*. *Proceedings of the National
803 Academy of Sciences* 116:19136–19144.
- 804 62. Gritsun DJ, Jones IM, Gould EA, Gritsun TS. 2014. Molecular archaeology of
805 Flaviviridae untranslated regions: duplicated RNA structures in the replication
806 enhancer of flaviviruses and pestiviruses emerged via convergent evolution. *PLoS
807 One* 9:e92056.
- 808 63. Łabno A, Tomecki R, Dziembowski A. 2016. Cytoplasmic RNA decay pathways -
809 Enzymes and mechanisms. *Biochimica et Biophysica Acta (BBA) - Molecular Cell
810 Research* 1863:3125–3147.
- 811 64. Chen Y-S, Fan Y-H, Tien C-F, Yueh A, Chang R-Y. 2018. The conserved stem-loop II
812 structure at the 3' untranslated region of Japanese encephalitis virus genome is
813 required for the formation of subgenomic flaviviral RNA. *PLoS One* 13:e0201250--17.
- 814 65. Akiyama BM, Laurence HM, Massey AR, Costantino DA, Xie X, Yang Y, Shi PY, Nix
815 JC, Beckham JD, Kieft JS. 2016. Zika virus produces noncoding RNAs using a multi-
816 pseudoknot structure that confounds a cellular exonuclease. *Science* (1979)
817 <https://doi.org/10.1126/science.aah3963>.
- 818 66. Bolling B, Weaver S, Tesh R, Vasilakis N. 2015. Insect-Specific Virus Discovery:
819 Significance for the Arbovirus Community. *Viruses* 7:4911–4928.
- 820 67. Qiu Y, Xu Y-P, Wang M, Miao M, Zhou H, Xu J, Kong J, Zheng D, Li R-T, Zhang R-R,
821 Guo Y, Li X-F, Cui J, Qin C-F, Zhou X. 2020. Flavivirus induces and antagonizes
822 antiviral RNA interference in both mammals and mosquitoes. *Sci Adv* 6.
- 823 68. Blair C, Olson K. 2015. The Role of RNA Interference (RNAi) in Arbovirus-Vector
824 Interactions. *Viruses* 7:820–843.
- 825 69. Lee W-S, Webster JA, Madzokere ET, Stephenson EB, Herrero LJ. 2019. Mosquito
826 antiviral defense mechanisms: a delicate balance between innate immunity and
827 persistent viral infection. *Parasit Vectors* 12:165.
- 828 70. Colmant AMG, Hobson-Peters J, Bielefeldt-Ohmann H, van den Hurk AF, Hall-
829 Mendelin S, Chow WK, Johansen CA, Fros J, Simmonds P, Watterson D, Cazier C,
- 830

- 831 Etebari K, Asgari S, Schulz BL, Beebe N, Vet LJ, Piyasena TBH, Nguyen H-D, Barnard
832 RT, Hall RA. 2017. A New Clade of Insect-Specific Flaviviruses from Australian
833 Anopheles Mosquitoes Displays Species-Specific Host Restriction. *mSphere* 2.
- 834 71. Rückert C, Prasad AN, Garcia-Luna SM, Robison A, Grubaugh ND, Weger-Lucarelli J,
835 Ebel GD. 2019. Small RNA responses of *Culex* mosquitoes and cell lines during acute
836 and persistent virus infection. *Insect Biochem Mol Biol* 109:13–23.
- 837 72. Fan Y-H, Nadar M, Chen C-C, Weng C-C, Lin Y-T, Chang R-Y. 2011. Small Noncoding
838 RNA Modulates Japanese Encephalitis Virus Replication and Translation in trans.
839 *Virol J* 8:492.
- 840 73. Alvarez DE, Lodeiro MF, Ludueña SJ, Pietrasanta LI, Gamarnik A V. 2005. Long-
841 Range RNA-RNA Interactions Circularize the Dengue Virus Genome. *J Virol* 79:6631–
842 6643.
- 843 74. Roby J, Pijlman G, Wilusz J, Khromykh A. 2014. Noncoding Subgenomic Flavivirus
844 RNA: Multiple Functions in West Nile Virus Pathogenesis and Modulation of Host
845 Responses. *Viruses* 6:404–427.
- 846 75. Clarke DK, Duarte EA, Elena SF, Moya A, Domingo E, Holland J. 1994. The red queen
847 reigns in the kingdom of RNA viruses. *Proceedings of the National Academy of
848 Sciences* 91:4821–4824.
- 849 76. Junglen S, Kopp A, Kurth A, Pauli G, Ellerbrok H, Leendertz FH. 2009. A New
850 Flavivirus and a New Vector: Characterization of a Novel Flavivirus Isolated from
851 Uranotaenia Mosquitoes from a Tropical Rain Forest. *J Virol* 83:4462–4468.
- 852 77. Bassett AR, Tibbit C, Ponting CP, Liu J-L. 2014. Mutagenesis and homologous
853 recombination in *Drosophila* cell lines using CRISPR/Cas9. *Biol Open* 3:42–49.
- 854 78. Afgan E, Baker D, Batut B, van den Beek M, Bouvier D, Čech M, Chilton J, Clements
855 D, Coraor N, Grüning BA, Guerler A, Hillman-Jackson J, Hiltemann S, Jalili V, Rasche
856 H, Soranzo N, Goecks J, Taylor J, Nekrutenko A, Blankenberg D. 2018. The Galaxy
857 platform for accessible, reproducible and collaborative biomedical analyses: 2018
858 update. *Nucleic Acids Res* 46:W537–W544.
- 859 79. de Borba L, Villordo SM, Marsico FL, Carballeda JM, Filomatori C V., Gebhard LG,
860 Pallarés HM, Lequime S, Lambrechts L, Sánchez Vargas I, Blair CD, Gamarnik A V.
861 2019. RNA Structure Duplication in the Dengue Virus 3' UTR: Redundancy or Host
862 Specificity? *mBio* 10.
- 863 80. Lorenz R, Bernhart SH, Höner zu Siederdissen C, Tafer H, Flamm C, Stadler PF,
864 Hofacker IL. 2011. ViennaRNA Package 2.0. *Algorithms for Molecular Biology* 6:26.
- 865 81. Katoh K, Standley DM. 2013. MAFFT Multiple Sequence Alignment Software Version
866 7: Improvements in Performance and Usability. *Mol Biol Evol* 30:772–780.
- 867 82. Criscuolo A, Gribaldo S. 2010. BMGE (Block Mapping and Gathering with Entropy): a
868 new software for selection of phylogenetic informative regions from multiple
869 sequence alignments. *BMC Evol Biol* 10:210.
- 870 83. Guindon S, Dufayard J-F, Lefort V, Anisimova M, Hordijk W, Gascuel O. 2010. New
871 Algorithms and Methods to Estimate Maximum-Likelihood Phylogenies: Assessing
872 the Performance of PhyML 3.0. *Syst Biol* 59:307–321.
- 873 84. Lemoine F, Correia D, Lefort V, Doppelt-Azeroual O, Mareuil F, Cohen-Boulakia S,
874 Gascuel O. 2019. NGPhylogeny.fr: new generation phylogenetic services for non-
875 specialists. *Nucleic Acids Res* 47:W260–W265.
- 876 85. Letunic I, Bork P. 2021. Interactive Tree Of Life (iTOL) v5: an online tool for
877 phylogenetic tree display and annotation. *Nucleic Acids Res* 49:W293–W296.

- 878 86. Brown NP, Leroy C, Sander C. 1998. MView: a web-compatible database search or
879 multiple alignment viewer. Bioinformatics 14:380–381.
880 87. Nicholson J, Ritchie SA, Van Den Hurk AF. 2014. *Aedes albopictus* (Diptera:
881 Culicidae) as a Potential Vector of Endemic and Exotic Arboviruses in Australia. J
882 Med Entomol 51:661–669.
883

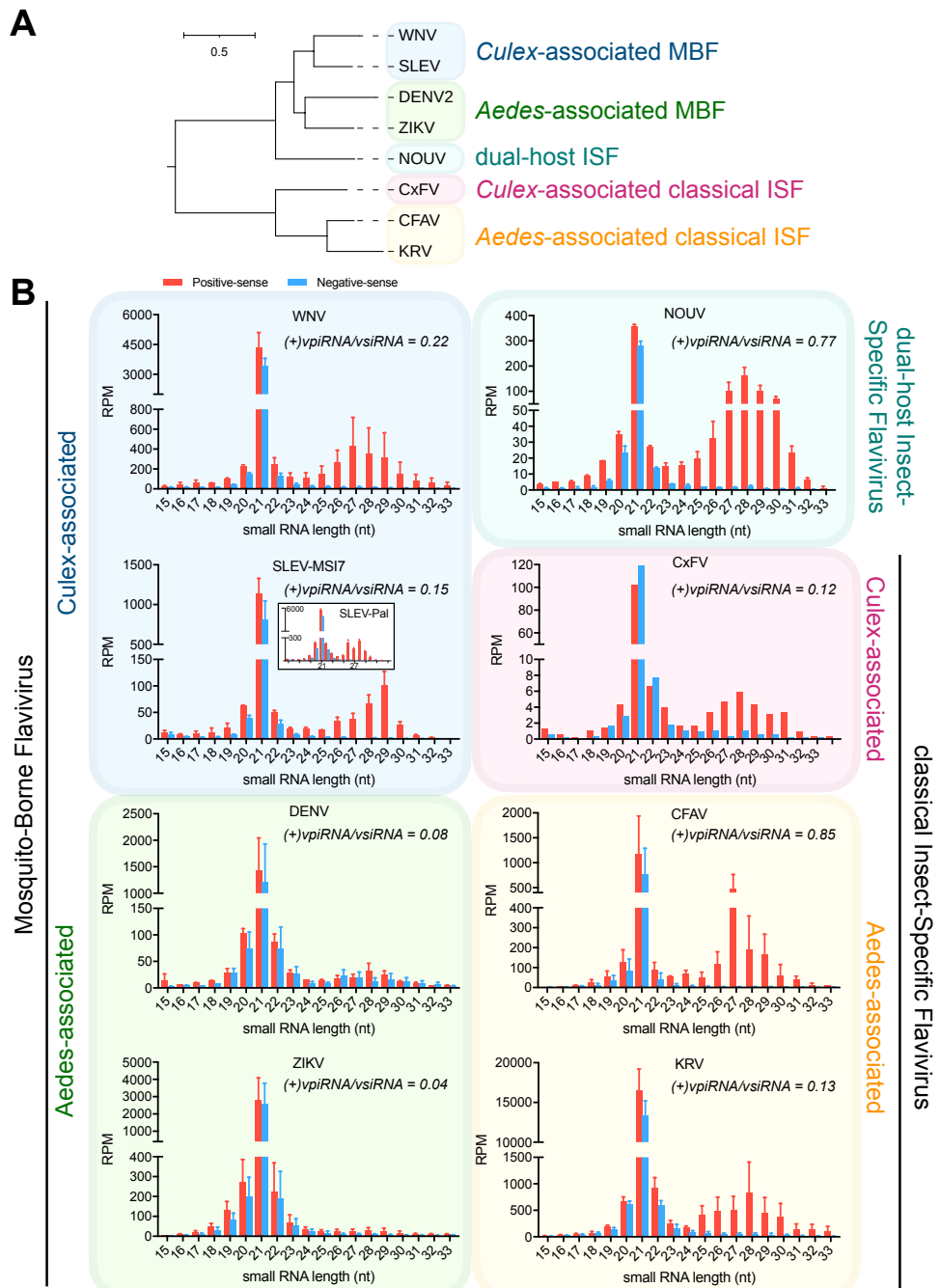
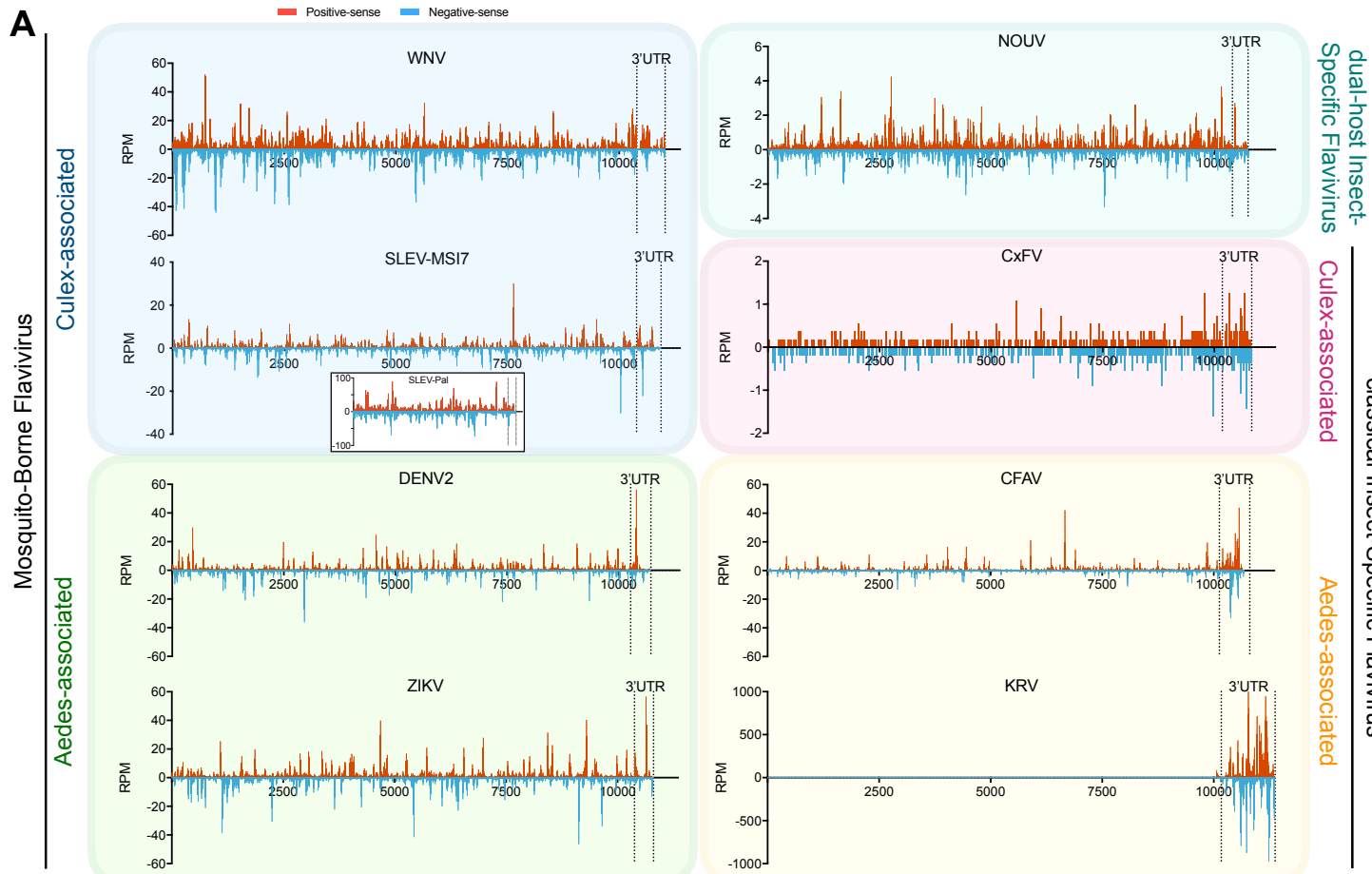
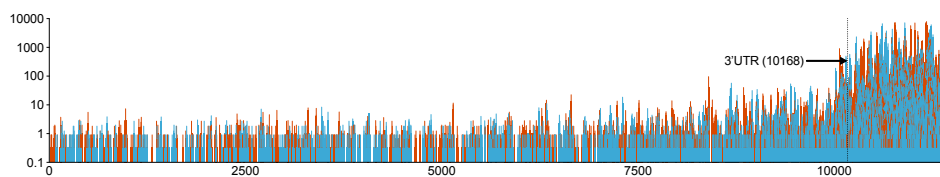
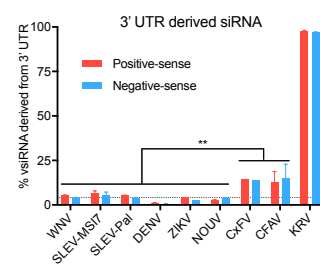


Fig. 1

A**B****C****Fig. 2**

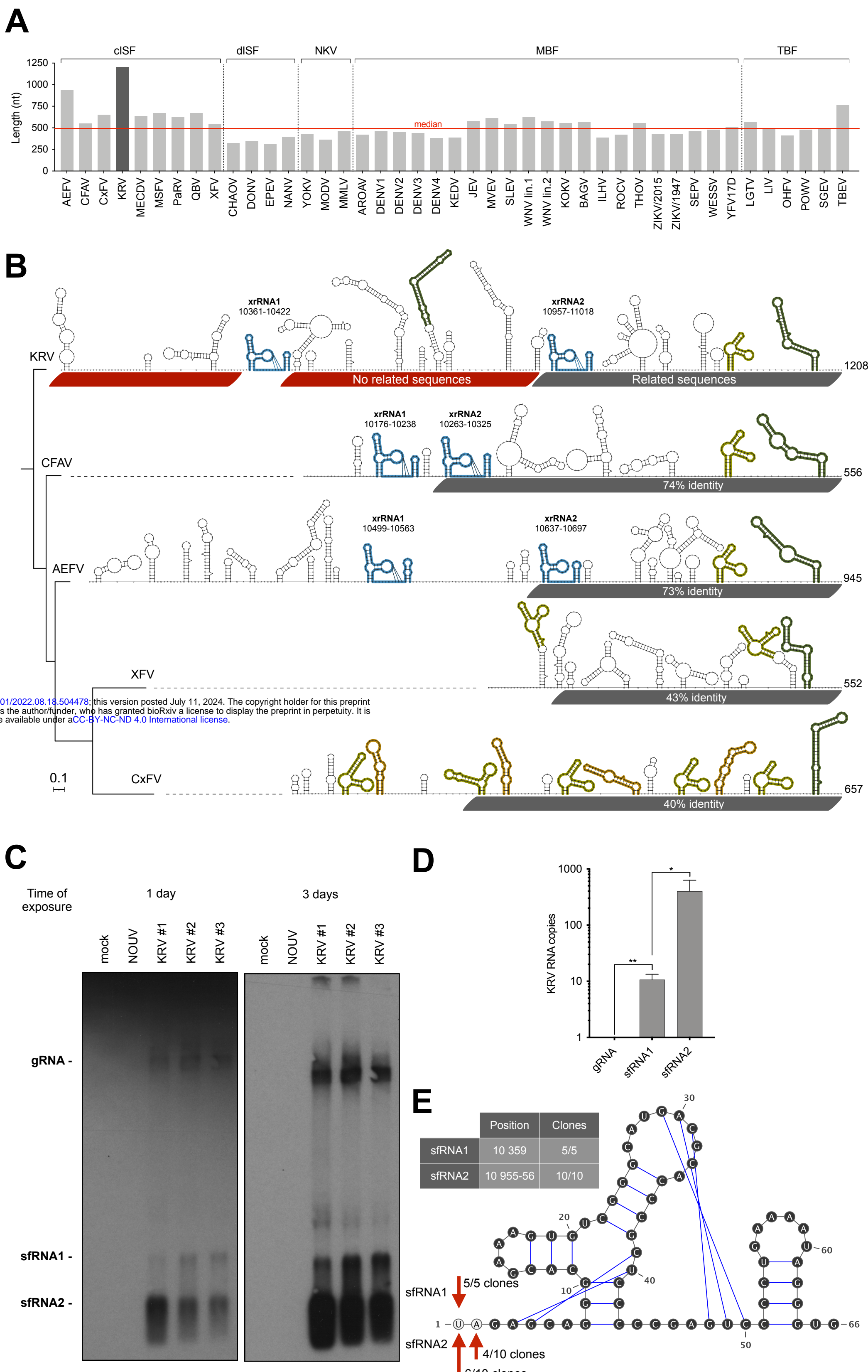


Fig. 3

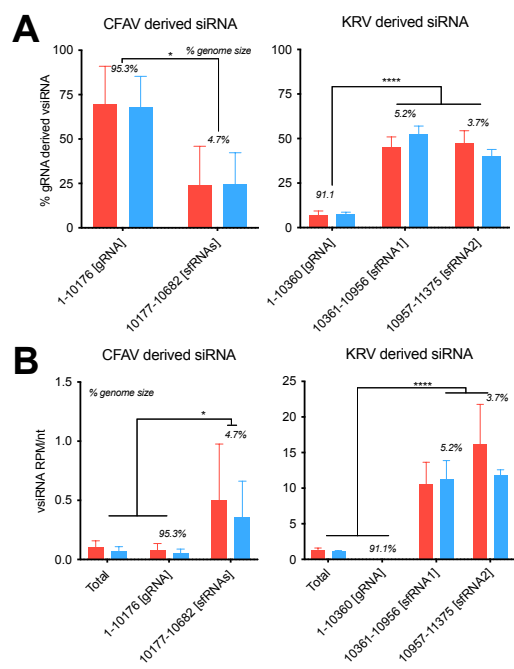


Fig. 4

Fig. 5

